Nutrient dose-responsive transcriptome changes driven by Michaelis–Menten kinetics underlie plant growth rates

Joseph Swift[a,1], Jose M. Alvarez[a,b,1], Viviana Araus[a], Rodrigo A. Gutiérrez[c], and Gloria M. Coruzzi[a,2]

[a]Center for Genomics and Systems Biology, Department of Biology, New York University, New York, NY 10003; [b]Centro de Genómica y Bioinformática, Facultad de Ciencias, Universidad Mayor, Santiago 8580745, Chile; and [c]Fondo de Desarrollo de Areas Prioritarias Center for Genome Regulation, Millennium Institute for Integrative Biology, Departamento de Genética Molecular y Microbiología, Pontificia Universidad Católica de Chile, Santiago 8331150, Chile

This contribution is part of the special series of Inaugural Articles by members of the National Academy of Sciences elected in 2019.

Contributed by Gloria M. Coruzzi, March 30, 2020 (sent for review October 25, 2019; reviewed by Julia Bailey-Serres and Nicolaus von Wiren)

An increase in nutrient dose leads to proportional increases in crop biomass and agricultural yield. However, the molecular underpinnings of this nutrient dose–response are largely unknown. To investigate, we assayed changes in the *Arabidopsis* root transcriptome to different doses of nitrogen (N)—a key plant nutrient—as a function of time. By these means, we found that rate changes of genome-wide transcript levels in response to N-dose could be explained by a simple kinetic principle: the Michaelis–Menten (MM) model. Fitting the MM model allowed us to estimate the maximum rate of transcript change (V_{max}), as well as the N-dose at which one-half of V_{max} was achieved (K_m) for 1,153 N-dose–responsive genes. Since transcription factors (TFs) can act in part as the catalytic agents that determine the rates of transcript change, we investigated their role in regulating N-dose–responsive MM-modeled genes. We found that altering the abundance of TGA1, an early N-responsive TF, perturbed the maximum rates of N-dose transcriptomic responses (V_{max}), K_m, as well as the rate of N-dose–responsive plant growth. We experimentally validated that MM-modeled N-dose–responsive genes included both direct and indirect TGA1 targets, using a root cell TF assay to detect TF binding and/or TF regulation genome-wide. Taken together, our results support a molecular mechanism of transcriptional control that allows an increase in N-dose to lead to a proportional change in the rate of genome-wide expression and plant growth.

nitrogen dose | Michaelis–Menten kinetics | transcriptome regulation

Due to their unique ability for indeterminate growth, plants can adapt their size and growth rate in response to the amount of nutrient available in their environment. Nitrogen (N) is a key nutrient that has such a dose-responsive effect on plant growth and development (1). For this reason, N-based fertilizers are routinely employed to enhance crop biomass and boost grain yields. However, such fertilizers are costly and harmful to the environment (2).

To help identify ways to improve plant N-use efficiency and reduce reliance on N fertilizers, the signaling mechanisms that allow plants to sense and respond to N availability are under intense scrutiny. Numerous transcriptome studies have detected an impressive catalog of genes that are differentially expressed in response to a change in N status, which participate in a wide range of biological processes related to growth and development (3–7). Together, these studies indicate that a large fraction of the plant genome, ∼10%, is transcriptionally responsive to N treatment.

Indeed, previous studies have shown that N nutrient dose sensing enables plants to reprogram both their gene expression patterns (8, 9) as well as their phenotype, including the rate of N uptake and plant growth (10, 11). However, what remains unknown are the molecular mechanisms that enable the dose of N to inform gene expression levels, and how such gene expression changes lead to dose-responsive changes in plant phenotype.

To address this question, we assayed transcriptome responses of *Arabidopsis thaliana* roots exposed to different N-doses over time. By modeling gene expression responses to N-dose as a function of time, we were able to reveal the in vivo kinetics that tailor gene expression responses to the dose of N available. By these means, we demonstrate that the dynamics of plant transcriptomic responses to N-dose follows simple kinetics, as described by the Michaelis–Menten (MM) model. While the MM model was designed to explain in vitro enzyme kinetics (12, 13), due to its simplicity it has enjoyed broad applicability (14, 15), including describing the rates of N uptake by plants and N-dose–dependent plant growth (10, 11). Using this model, we found that the rate of transcript accumulation is a function of N-dose, which reached a saturation point at the highest N-doses tested.

Significance

How organisms sense and respond to changes in nutrient dose is a basic unanswered question that is relevant to agriculture. Here, we demonstrate that genome-wide expression levels in the *Arabidopsis* root are nutrient dose-responsive. We find that such dose-responsive gene expression patterns are driven largely by Michaelis–Menten (MM) kinetics, indicating that genome-wide transcriptional responses to nutrient dose resemble a simple principle of enzyme kinetics. Transcription factors (TFs) can act as "catalysts" driving rates of transcript change in response to nutrient dose. Supporting this, we identified TGA1 as a TF that controls nitrogen-dose–dependent rates of transcriptional change and plant growth. Thus, our study of the molecular mechanisms that underlie N-dose–responsive transcriptome kinetics could lead to enhanced crop growth.

Author contributions: J.S., J.M.A., R.A.G., and G.M.C. designed research; J.S., J.M.A., and V.A. performed research; J.S. and J.M.A. analyzed data; and J.S., J.M.A., and G.M.C. wrote the paper.

Reviewers: J.B.-S., University of California, Riverside; and N.v.W., Leibniz-Institute for Plant Genetics and Crop Plant Research.

The authors declare no competing interest.

Data deposition: The raw sequencing data reported in this paper have been deposited in the National Center for Biotechnology Information Sequence Read Archive (accession no. PRJNA522060). Vectors are available from National Center for Biotechnology Information (accession no. MN991175).

[1]J.S. and J.M.A. contributed equally to this work.

[2]To whom correspondence may be addressed. Email: gloria.coruzzi@nyu.edu.

This article contains supporting information online at https://www.pnas.org/lookup/suppl/doi:10.1073/pnas.1918619117/-/DCSupplemental.

The MM model predicts the rate at which a catalyst can convert a substrate to its product. By analogy, transcription factors (TFs) act in part as the "catalyst" that drive rates of transcript change. To test this, we investigated whether altering TF abundance *in planta* could impact the maximum rate at which transcript abundance changed (V_{max}) in responses to N-dose. We show that the overexpression of the TF TGA1 (*TGACG SEQUENCE-SPECIFIC BINDING PROTEIN 1*) leads to an increase in the maximum rate of transcript change in response to N-dose (V_{max}), as predicted by the MM model. Furthermore, we validated TGA1's direct gene targets genome-wide through RNA sequencing (RNA-seq), chromatin immunoprecipitation sequencing (ChIP-seq), and 4-thiouracil (4tU) labeling of nascent transcripts, revealing that TGA1 directly regulates both N-metabolic genes and their TF regulators. Importantly, we show that TGA1's impact on the kinetics of the N-dose–response at the molecular level leads to an acceleration in N-dependent plant growth rates. In this way, our study of the basic mechanisms that underlie the transcriptome kinetics responding to changes in N-dose could potentially enhance plant growth and improve N-use efficiency.

Results

N-dose Informs Rates of Transcript Change Genome-Wide in *Arabidopsis* Roots. To understand the transcriptional mechanisms underlying plant responses to N-dose, we assayed how the *Arabidopsis* transcriptome responds to N-dose as a function of time. To achieve this, we treated hydroponically grown, wild-type *Arabidopsis* seedlings to four increasing doses of N (0, 1, 10, and 60 mM N, provided as KNO_3 + NH_4NO_3) over five time points (15, 30, 60, 120, and 240 min) (Fig. 1*A*). The maximum N-dose used reflected the amount of N present in standard Murashige and Skoog (MS) plant growth media (16). The time points were selected to capture the early transcriptional events that occur in response to N sensing (5). This experimental setup generated a factorial matrix holding 20 unique treatment conditions (Fig. 1*A*). For each condition, we harvested the root tissue of ∼30 plants and assayed their transcriptome by RNA-seq.

To identify genes differentially expressed in response to N-dose as a function of time, we fit normalized gene expression patterns with a linear model. This model was designed to detect genes that were either responsive to the dose of N provided (N), time (T), or the interaction between the two (N×T) (Fig. 1*B*). We employed model simplification to determine the best linear model that explained each gene's expression. After excluding genes that were time-responsive only—and thus not relevant to our study—we found 4,938 genes that were differentially expressed as a function of N (adjusted $P < 0.01$) (Fig. 1*B* and *SI Appendix*, Table S1). We found that 77% of these N-dose–response genes (3,818 genes) were explained by a model holding an N×T interaction term, indicating that the majority of genes that responded to N-dose did so as a function of time (Fig. 1*B*). Among these were well-known genes involved in N transport and assimilation such as the *NITRATE TRANSPORTER 1.1* (NRT1.1/NPF6.3), *NITRATE REDUCTASE 1* (NIA1), *GLUTAMINE SYNTHETASE* (GLN1), *ASPARTATE AMINOTRANSFERASE* (ASP3), and *GLUTAMATE DEHYDROGENASE* (GDH3) (*SI Appendix*, Table S1). Genes that were modeled by an N×T interaction term included many known N-responsive genes found through previous transcriptomic analyses (*SI Appendix*, Fig. S1), suggesting that many previously reported N-responsive genes are N-dose responsive.

To further understand how the expression of these 3,818 "N×T" genes was governed by both N-dose and time (T), we performed a fold-change analysis. To do this, we counted how many genes regulated at each time-point passed a ±1.5-fold change cutoff. This revealed that a higher N-dose led to more genes being differentially expressed at earlier time points (Fig. 1*A*). We next asked whether higher doses of N lead to higher

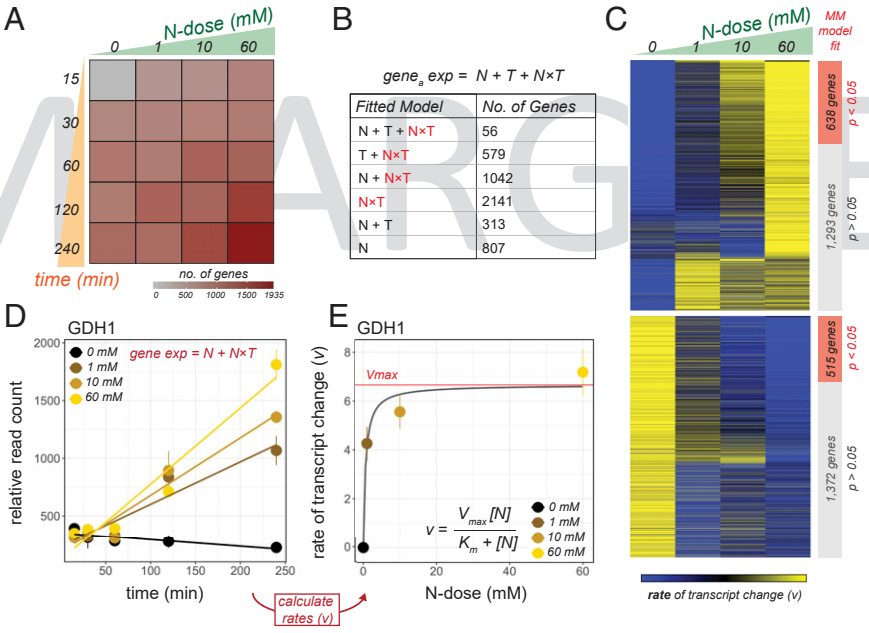

Fig. 1. Michaelis–Menten (MM) kinetics underlie transcriptomic responses to N-dose in *Arabidopsis* roots. (*A*) A factorial treatment matrix systematically varied both the exposure time to N and the N-dose provided. Colors indicate how many genes were differentially expressed (fold change cutoff ± 1.5) in response to N-dose in each condition. (*B*) Differentially expressed genes were detected using a multivariate linear model. Seventy-seven percent of genes found by linear modeling (3,818 genes) were fit by a model holding an N×T term. (*C*) Heatmap displaying rates of transcript change for each of the 3,818 genes under each N-dose. Genes whose rate change in N-dose–responsive expression significantly fit the MM model (1,153 genes) are indicated in red. (*D*) GDH1 is an example of a gene fit by model holding a "N×T" term. (*E*) GDH1 is also an example of a gene whose rate of N-dose–responsive expression is significantly fit by the MM model.

rates of transcript change for each gene. To answer this, we calculated the change in each gene's transcript abundance over time under each N-dose. Each rate was calculated by fitting a linear model to each N-dose tested (*Materials and Methods*). Comparing these rates revealed a genome-wide trend; we found that genes displayed rates of transcript change that either increased or decreased in proportion to the dose of N provided (Fig. 1*C*). An example of a gene that fits this trend is the N-assimilation gene *GLUTAMATE DEHYDROGENASE 1* (GDH1) (Fig. 1*D*).

Next, we assessed whether such transcriptome responses to N-dose fit a general biological model that describes how reaction rates change. Specifically, we tested whether the rate changes in transcript levels could be explained by MM kinetics (12, 13). To do this, we fit each gene's expression pattern to the MM model (*Materials and Methods*). A gene significantly fit by this MM model allowed us to estimate the maximum rate of transcript change (V_{max}), as well as the dose of N at which one-half of V_{max} was achieved (K_m). We found that the MM kinetic model was able to explain the expression responses of 1,153 N-dose responsive genes (adjusted $P < 0.05$; *SI Appendix*, Table S2), including GDH1 (Fig. 1 *D* and *E*). Additionally, we found that the MM model was able to describe genes either activated or repressed by N-dose (Fig. 1*C*). The significant gene ontology (GO) terms enriched in up-regulated genes included "response to abiotic stimulus" and "response to inorganic substance" (*SI Appendix*, Table S3). Moreover, our MM modeling approach indicated that at a N-dose of 60 mM, many genes were being induced or repressed close to their estimated maximum rate (V_{max}).

Transcription Factor TGA1 Regulates Transcriptional Response Rates to N-dose. According to the MM model, changing enzyme abundance will impact the maximum rate of reaction possible (V_{max}). TFs likely serve as the main catalyst driving rates of transcript change in response to N-dose. To assess the robustness of our MM models, as well as identify TFs that signal N-dose, we sought to test how altering TF abundance could perturb N-dose transcriptomic responses, with the goal of observing whether their V_{max} estimates change.

We took two complementary approaches to identify candidate TFs responsible for mediating the rates of transcriptional change in response to N-dose. First, we investigated the expression patterns of TFs regulated by N-dose as a function of time within our experiment. We hypothesized that TFs that responded early might be involved in governing N-dose–responsive transcription. We thus ranked all expressed TFs within the *Arabidopsis* genome by their fold change in response to N-dose at the earliest time point tested (15 min) (Fig. 2*A*). Of these, the top three early N-dose–responsive TFs were *LOB DOMAIN-CONTAINING PROTEIN 37* (LBD37), LBD38, and TGA1, with 32-, 20-, and 18-fold change in gene expression, respectively (Fig. 2*A* and *SI Appendix*, Fig. S2). All three TFs have been previously implicated in transcriptional regulation of N-responsive genes *in planta* (17, 18). Second, we searched for overrepresented *cis*-regulatory elements in the promoters of the 1,153 genes whose expression in response to N-dose could be explained by the MM model (Fig. 1*C*). We found that the TGA1 binding site was significantly overrepresented in the genes whose N-dose–responsive expression could be modeled by MM kinetics (Fig. 2*B*). Moreover, we found that genes whose N-dose–response is modeled by MM kinetics are preferentially expressed within inner cell layers of the root (pericycle and stele), where TGA1 itself is expressed (18, 19) (*SI Appendix*, Fig. S3).

Together, these findings suggested that TGA1 is a TF involved in regulating transcriptional responses to N-dose. To

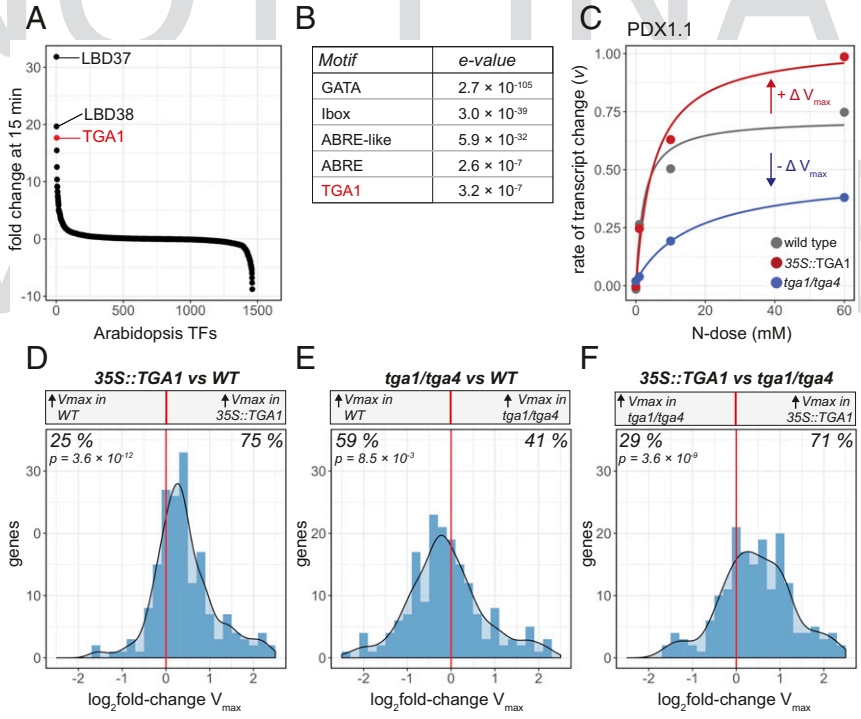

Fig. 2. N-dose–response rates of transcripts mediated by changes in TGA1 levels *in planta*. (*A*) A ranking in expression fold change for mRNAs of all plant TFs after 15 min of exposure to N treatment. (*B*) *cis*-regulatory analysis identifies overrepresented motifs among the 1,153 N-dose–responsive genes captured by the MM model. (*C*) Changes in N-dose–dependent transcription rate of PDX1.1 is fit by the MM model in wild type, and V_{max} is altered in the *35S::*TGA1 and *tga1/tga4* lines. (*D–F*) A histogram of $\log_2$ fold changes in V_{max} shown for 192 MM-modeled genes up-regulated by N-dose across wild-type and TGA1 genotypes. *D* compares these changes in V_{max} between *35S::*TGA1 and wild type; *E*, between *tga1/tga4* and wild type; and *F*, between *35S::*TGA1 and *tga1/tga4*. A binomial test was used to assess bias toward an increase or decrease in V_{max}.

test this hypothesis, we repeated our factorial matrix experiment that varied N-dose over time (Fig. 1*A*), but now assessing the transcriptomic responses of a TGA1-overexpressing line (*35S::*TGA1) (20) and a *tga1*/*tga4* double mutant (18). We note it was necessary to use the *tga1*/*tga4* mutant line, as TGA4 is the closest gene homolog to TGA1, and as such these TFs have been shown to act redundantly (18). Our results indicated that overexpression of TGA1 *in planta* led to increases in rates of transcriptional change in response to N-dose (Fig. 2 *D* and *F*), while knocking out TGA1 and TGA4 led to decreased rates of transcriptional change (Fig. 2 *E* and *F*). This effect was captured by fitting the MM model to gene expression patterns in the *35S::*TGA1 and *tga1*/*tga4* lines to estimate V_{max}, and comparing these V_{max} estimates to those of wild type (Fig. 2). Of the 192 genes we were able to significantly model using MM kinetics in all three genotypes (wild type, *35S*::TGA1, *tga1*/*4*) (adjusted $P < 0.05$), we found that 75% of these genes held higher V_{max} values when TGA1 was overexpressed (*35S::*TGA1) (Fig. 2*D* and *SI Appendix*, Table S2). GO terms for genes with higher V_{max} estimates in the TGA1-overexpressing lines included "translation," "glucose metabolic process," and "generation of precursor metabolites and energy" (*SI Appendix*, Table S2). In addition to these 192 MM-modeled genes, we also observed higher V_{max} values for all N–up-regulated genes in the TGA1-overexpressing line, even if their resulting model *P* value did not pass the significance threshold (*SI Appendix*, Fig. S4). This suggested higher expression of TGA1 leads to increased rates of transcriptional change (i.e., increased V_{max}) in response to changes in N-dose. This was further supported through conducting the same analysis in the *tga1*/*tga4* knockout line, where V_{max} estimates for these genes were found to be lower compared either to wild-type or the *35S*::TGA1 line (Fig. 2 *E* and *F* and *SI Appendix*, Fig. S4). An example of a gene fitting this expression pattern is illustrated in Fig. 2*C*, where the MM model explains the rates of transcript change of *PYRIDOXINE BIOSYNTHESIS 1.1* (PDX1.1), a glutamine amidotranferase (21), within each genotype. Here, the *35S::*TGA1 line held a higher V_{max} estimate compared to wild type, while the *tga1*/*tga4* mutant line held a lower V_{max} estimate. Changing levels of TGA1 *in planta* also impacted V_{max} estimates for GDH1, in a similar fashion to PDX1.1 (*SI Appendix*, Fig. S5). Collectively, these data support the conclusion that TGA1 acts as transcriptional activator, increasing transcriptional response rates to N-dose. This is further supported by our finding that perturbing levels of TGA1 expression had a weaker effect on genes down-regulated by N (*SI Appendix*, Fig. S6).

Additionally, for MM-modeled genes that were up-regulated by N-dose genome-wide, we found a global increase in K_m estimates within both the *tga1*/*tga4* mutant and in the *35S::*TGA1 lines, relative to wild type (*SI Appendix*, Fig. S7). Specifically, in the *tga1*/*tga4* mutant background, not only were the majority of estimated maximum rates of transcriptional change (V_{max}) lower relative to wild type (Fig. 2*E*), but the N-dose required to achieve half the maximum rate (K_m) increased (*SI Appendix*, Fig. S7*B*). For the *35S::*TGA1 line, the K_m estimates also increased (*SI Appendix*, Fig. S7*A*). Since the estimated maximum rate of transcriptional change (V_{max}) was higher in the *35S::*TGA1 background (Fig. 2*D*), the N-dose required to reach this higher rate of transcriptional change is reflected in an increase in K_m (*SI Appendix*, Fig. S7*A*). The response of gene ATDF2, encoding a ferredoxin-like superfamily protein, illustrates how K_m values can increase when TGA1 is overexpressed (*35S::*TGA1), as well as when it is absent (*tga1*/*tga4*) (*SI Appendix*, Fig. S7*D*).

TF-Perturbation Assays Uncover TGA1 as a Transcriptional Activator in Root Cells. Our transcriptomic analysis identified genes whose response to N-dose is mediated by TGA1 *in planta*; overexpression of TGA1 showed increased rates of transcript change relative to wild-type plants (Fig. 2 *C*–*F*). To experimentally determine whether this is a direct result of transcriptional activation by TGA1, we used the plant cell-based TARGET TF-perturbation assay, which can identify direct, actively transcribed targets of a TF (22). To perform this assay, we transiently expressed TGA1 in root protoplasts as a TGA1 glucocorticoid receptor fusion protein (TGA1-GR). To control TF import into the nucleus, transfected root cells expressing TGA1-GR were sequentially treated with 1) +/− N, 2) cycloheximide (+/− CHX), and 3) dexamethasone (+/− DEX) (Fig. 3*A* and *Materials and Methods*). DEX treatment induces nuclear import of the TGA1-GR fusion protein (23). Genes regulated by DEX-induced TF import are deemed direct "primary" targets of TGA1, since a +CHX pretreatment blocks translation of downstream regulators (22, 24). N treatment is included to induce any post-translational modifications of TGA1 (25) or influence TGA1 partners by transcriptional or posttranscriptional mechanisms.

Through analysis of mRNA-seq data, we identified 584 direct gene targets of TGA1 in root cells (adjusted $P < 0.05$), 77% of which were up-regulated by TGA1 nuclear import, a higher proportion than expected by chance (binomial test, $P = 9 \times 10^{-40}$) (Fig. 3*B* and *SI Appendix*, Table S4). This provided evidence that TGA1 serves largely as a transcriptional activator. Additionally, genes up-regulated by TGA1 held higher significance values and greater fold-change differences than down-regulated genes (*SI Appendix*, Fig. S8*A*). Among the direct regulated targets of TGA1 were N-related genes *AMMONIUM TRANSPORTER 1.3* (AMT1.3), *GLUTAMATE SYNTHASE 1* (GLT1), *GLUTAMATE SYNTHASE 2* (GLU2), and *GLUTAMATE DECARBOXYLASE* (GAD4) (*SI Appendix*, Table S4). In line with this, GO terms enriched in TGA1 direct targets were related to metabolism including "regulation of cellular metabolic process" and "regulation of nitrogen compound metabolic process" (*SI Appendix*, Table S5).

To confirm that TGA1 directly initiates the transcription of its 584 direct targets as identified by mRNA-seq, we also tracked de novo synthesis of mRNAs made in response to TGA1 nuclear import. To do this, we repeated our TARGET TF-perturbation experiment, but spiked the isolated root cells with 4tU after DEX-induced nuclear import of TGA1, as described in ref. 26 (Fig. 3*A*). 4tU is a uracil analog that is incorporated into nascent mRNA transcripts, which can then be selectively isolated using a streptavidin mediated pull-down assay (27). Thus, we used 4tU to label, affinity purify, and sequence de novo transcripts that were actively transcribed in response to TGA1 nuclear localization (26). Using 4tU, we validated that TGA1 nuclear import resulted in de novo transcription of 83% of TGA1's 584 direct targets (*SI Appendix*, Table S4). In addition, the magnitude of de novo transcript synthesis in response to TGA1 nuclear import correlated with the magnitude of steady-state mRNA levels ($R = 0.82$) (*SI Appendix*, Fig. S8*B*). This result indicates that active transcriptional regulation by TGA1 can largely explain changes in target gene transcript levels.

Next, we aimed to detect TGA1-DNA binding events in root cells using the TARGET assay. To do this, we employed ChIP-seq, using anti-GR antibodies against the TGA1-GR fusion protein (28). The aggregate binding profile of gene targets bound by TGA1 in root cells shows that TF binding occurs close to the transcription start site as well as the transcription termination site (*SI Appendix*, Fig. S9 and Table S4). We found a significant overlap between genes found bound by TGA1 and target genes directly regulated by TGA1 (*SI Appendix*, Fig. S8*C*). We also found a significant overlap between genes bound to TGA1 by ChIP-seq, and those bound to TGA1 as assayed by in vitro DNA affinity purification sequencing (DAP-seq) (29) (*SI Appendix*, Fig. S8*C*).

Combined, our mRNA-seq, 4tU, and ChIP-seq experiments allowed us to detect gene targets that TGA1 both binds to and actively regulates. For example, the *NODULE INCEPTION*

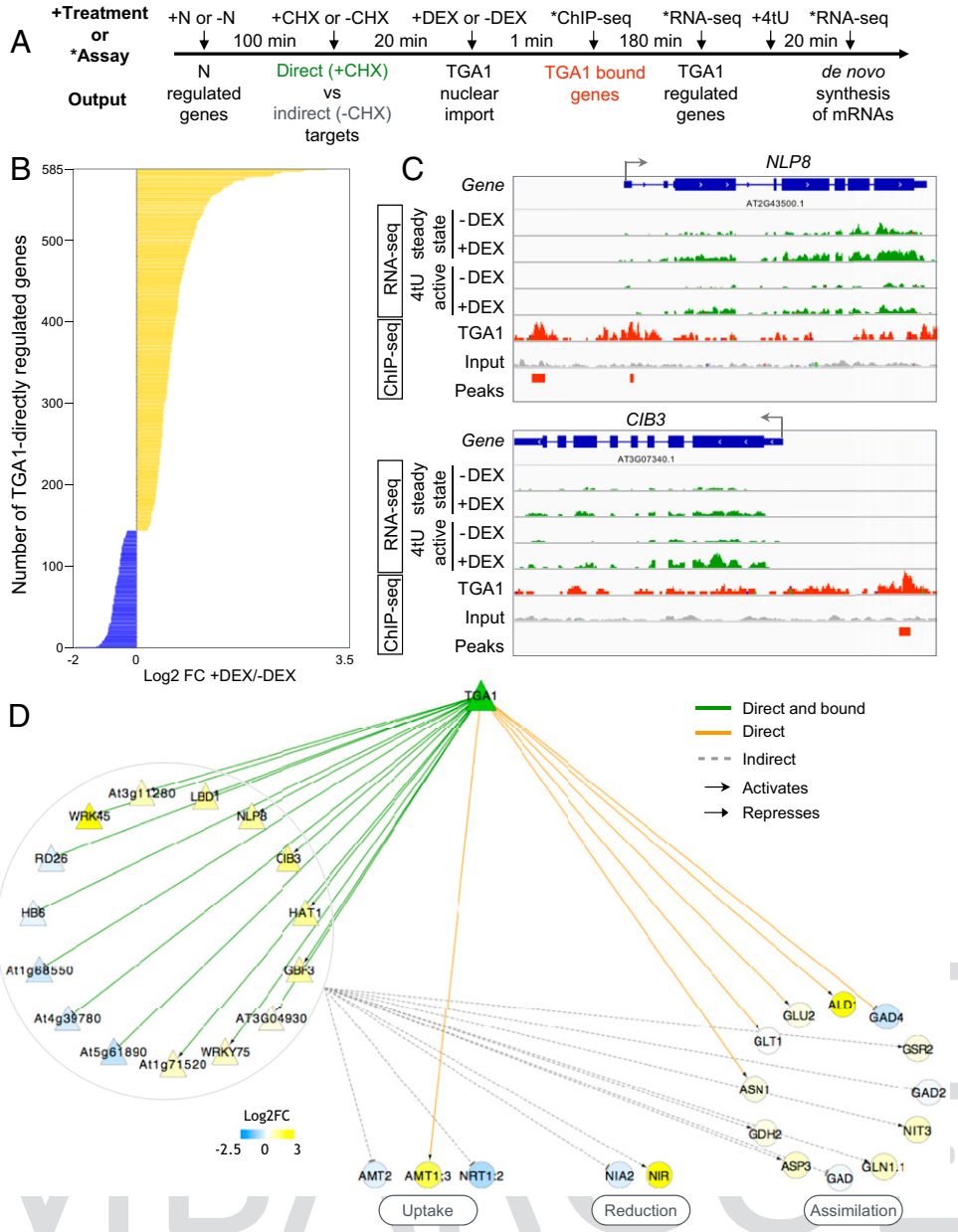

Fig. 3. TGA1 is a transcriptional activator that regulates both TFs and N-uptake/assimilation genes in root cells. (*A*) Workflow of TARGET TF-perturbation assay that can detect the gene targets that TGA1 binds to and regulates in isolated root cells. (*B*) The TARGET TF-perturbation assay reveals TGA1 directly up-regulates (yellow, 77%) or down-regulates (blue, 23%) the expression of 584 genes in root cells (*SI Appendix*, Table S4). (*C*) NLP8 and CIB3 TFs are examples of direct targets transcriptionally activated by TGA1. The expression of NLP8 and CIB3 is affected by TGA1 nuclear import, as assayed by both RNA-seq (steady-state mRNA) and by 4tU affinity capture (de novo mRNA) (green bars). TGA1 binding at these loci was captured by ChIP-seq (red bars). (*D*) TGA1 transcriptional subnetwork in root cells, where nodes represent genes and edges represent regulatory interactions detected by our assay. TGA1 directly or indirectly—through intermediate TFs (triangles)—regulate the expression genes involved in N uptake/metabolism (circles).

PROTEIN 8 (NLP8) and *CRY2-INTERACTING bHLH 3* (CIB3) TFs were among genes bound to and directly regulated by TGA1. NLP8 has been previously implicated in regulating N-promoted seed germination (30), while CIB3 has been previously implicated in light signaling (31) (Fig. 3*B*). The expression of both genes was induced by TGA1 nuclear import under +CHX treatments, indicating that NLP8 and CIB3 are primary TGA1 targets. ChIP-seq confirmed TGA1 binding in the promoter of NLP8 and CIB3, and the 4tU labeling showed that both genes were actively transcribed due to TGA1 binding (Fig. 3*B*).

From these datasets, we found that TGA1 directly regulates a large number of TFs (92 TFs out of 584 TGA1 direct targets, 16%). Indeed, the GO term "regulation of transcription" was significantly enriched among the 584 direct targets of TGA1 ($P = 0.02$) (*SI Appendix*, Table S5). The large amount of TFs directly controlled by TGA1 suggests that a main function of TGA1 is to induce a transcriptional cascade. To characterize the downstream effects of TGA1, we performed our TARGET TF-perturbation experiment without blocking protein translation (i.e., in the absence of CHX). This allowed us to also detect gene expression responses that were downstream of TGA1's direct TF targets (Fig. 3*A*). We identified a total of 2,280 "indirect" targets of TGA1, defined as genes that are regulated by DEX-induced nuclear import of TGA1 under −CHX conditions, but not in

+CHX conditions (*SI Appendix*, Table S4). GO term enrichment analysis of TGA1 indirect targets included "response to nutrient levels" and "growth." To make sense of how the direct and indirect targets of TGA1 identified in root cells impact the expression of genes involved in N uptake and assimilation, we built a TF network (Fig. 3*C*). We used Cytoscape (32) to visualize the resulting network that included 32 genes in the N-uptake/assimilation pathway that are downstream targets of TGA1. This network revealed two modes of action of TGA1 on the N-uptake/assimilation pathway. First, TGA1 directly regulates the expression of *AMMONIUM TRANSPORTER 1.3* (AMT1.3), *GLUTAMATE SYNTHASE 1* (GLT1), *GLUTAMATE SYNTHASE 2* (GLU2), *GLUTAMATE DECARBOXYLASE* (GAD4), and *ASPARAGINE SYNTHASE 1* (ASN1). Second, through the regulation of secondary TFs, TGA1 indirectly influences the expression of additional N-uptake/assimilation genes, such as *NITRATE TRANSPORTER 1.2* (NRT1.2), *NITRATE REDUCTASE 2* (NIA2), *NITRITE REDUCTASE* (NIR), and *ASPARTATE AMINOTRANSFERASE 3* (ASP3) (Fig. 3*C*).

Importantly, through repeating our TARGET TF-perturbation experiments in root cells isolated from the *tga1/tga4* mutant, we found that the absence of TGA4 did not impact the regulation of TGA1 direct or indirect targets, as identified by regulated TGA1 nuclear import (*SI Appendix*, Fig. S10). This suggests that TGA1 and TGA4 are functionally redundant in N-signaling responses, in agreement with previous reports (18).

Last, we investigated the extent to which this TGA1 regulated gene network identified in root cells captured genes whose N-dose–responsive expression was explained by the MM model *in planta* (Fig. 1*C*). We found a significant overlap of both direct and indirect targets of TGA1 with genes whose N-dose–dependent expression rates fit the MM model *in planta* (*SI Appendix*, Fig. S8*C*). In line with TGA1 acting as an activator of gene expression, we found that the majority of TGA1 direct targets held higher V_{max} estimates in the *35S::*TGA1 line compared to wild type (*SI Appendix*, Fig. S8*D*). We found that the majority of TGA1 downstream indirect targets also held higher V_{max} estimates, suggesting that TGA1 impacts rates of N-dose–dependent gene expression through secondary TFs.

TGA1 Levels Mediate Accelerated *Arabidopsis* Growth Rates in Response to N-dose. Since we found evidence that TGA1 plays a role in regulating rates of transcription in response to N-dose, including the regulation of N-uptake/assimilation genes, we next investigated TGA1's effect on plant phenotype under increasing N-dose treatments. To do this, we examined how wild-type plants, the *35S::*TGA1-overexpressing line, and the *tga1/tga4* double-knockout mutant line grew in response to four different N doses (0.1, 1, 10, and 60 mM N, provided as KNO_3 + NH_4NO_3). By sampling whole-plant dry weight 6, 9, 12, and 15 d after sowing, we found that levels of TGA1 expression impacted plant growth rates in response to N-dose (Fig. 4 *A–F* and *I*).

Compared to wild type, overexpression of TGA1 led to significantly higher growth rates and increased biomass (three-way ANCOVA, $P = 4.1 \times 10^{-5}$). This effect was dependent on N dose; higher rates of growth were achieved with higher doses of N. At the highest N-dose of 60 mM, *35S::*TGA1 plants grew three times faster than wild type, reaching a dry weight that was 2.8 times greater (Fig. 4 *C* and *F* and *SI Appendix*, Fig. S11). This result was confirmed using an independent transgenic line of *35S::*TGA1 (*SI Appendix*, Fig. S11). Consistent with these findings, the *tga1/tga4* mutant grew 2.9 times slower compared to wild type, with a final dry weight that was 2.1 times smaller ($P = 1.5 \times 10^{-7}$) (Fig. 4 *B* and *E* and *SI Appendix*, Fig. S11).

We also assayed the root transcriptomes of wild-type and *35S::*TGA1 plants grown under the N-dose conditions described above. By these means, we found evidence that TGA1's ability to accelerate plant growth was associated with changes in expression of TGA1 gene targets. Specifically, the N-dose–response of 1,398 genes were significantly perturbed in the *35S::*TGA1 background, as identified by two-way ANCOVA analysis (*SI Appendix*, Fig. S11 and Table S6). Among these genes were known N-assimilation genes such as *GLUTAMATE SYNTHASE* (GLU1), which displayed a higher N-dose–response in the *35S::*TGA1 line (Fig. 4*G*). We found that these 1,398 genes whose N-dose–response was perturbed in the *35S::*TGA1 line significantly intersected with genes characterized as direct or indirect targets of TGA1, or whose N-dose expression was explained by MM kinetics (Fig. 4*H*). Collectively, these results suggest TGA1's influence on transcription rates of target genes at the molecular level translates to increased rates of growth in response to N-dose.

Discussion

As key nutrient, N has a dose-responsive effect on plant growth and development. Indeed, N-dose–responsive traits, including the rate of N uptake as well as the rate of N-responsive plant growth, have been shown to follow MM kinetics (Fig. 5 *A* and *C*) (10, 11). However, the molecular mechanisms that align the rate of N uptake with the rate of N-mediated changes in plant growth have remained poorly understood. Results presented herein help bridge this gap. Specifically, we show that N-dose–responsive transcriptome changes driven by MM kinetics underlie changes in plant growth rate. Additionally, we identify TGA1 as a TF involved in mediating this N-dose– response (Fig. 5*B*).

Previous studies have shown that mRNA responses of individual genes to changes in endogenous or exogenous signals can be explained by the MM model (33, 34). Herein, we found the MM model could explain transcriptome-wide transcriptional changes in response to N-dose. Specifically, for 30% of all N-dose–responsive genes (1,153 genes), we found that the rates at which they respond transcriptionally to N-dose could be explained by MM kinetics (Fig. 1). Importantly, MM model revealed the relationship between N-dose and rates of transcriptional change was not linear—higher doses of N had diminishing effects on the rate at which genes were induced or repressed. This effect is similar to what occurs in in vitro enzymatic reactions the MM model describes; the rate of the reaction will peak at saturating levels of substrate (35). Likely, the expression of the remaining 70% of N-dose–responsive genes that were not explained by the MM model were driven by more complex kinetics. For example, such genes may be influenced by both activating and repressing TFs, resulting in more complex patterns of expression. This is supported by previous reports showing multiple TFs can target the same N-responsive gene (20, 36). Additionally, such transcripts may hold distinct mRNA degradation rates, or be impacted by posttranscriptional regulatory mechanisms (37, 38); parameters that are not included in the MM model.

Modeling transcriptome kinetics led us to identify TGA1 as a candidate TF involved in establishing rates of transcript change in response to N-dose (Fig. 2). This was based on TGA1's early N-dose–responsive expression, and the enrichment of its *cis*-binding motif within the 1,153 genes whose N-dose–response fit the MM model. By modeling the kinetics of transcript change, we found that increasing levels of TGA1 *in planta* can increase the maximum rate of gene expression (V_{max}). This agrees with the MM model, where an increase in the amount of catalyst—in our case, a TF—allows for higher rates of reaction (V_{max}) to occur. By illustrating in vivo and genome-wide that the catalytic effects a TF can have on transcription rates follows this simple kinetic principle, we provide biological context to TF kinetic properties that are absent from in vitro assays of TF–target binding.

We note that within our MM modeling, the parameters of V_{max} and K_m not only depend on the transcriptional activity of TGA1, but are also informed by additional gene regulatory mechanisms, including other TFs. This is exemplified by N-dose–dependent

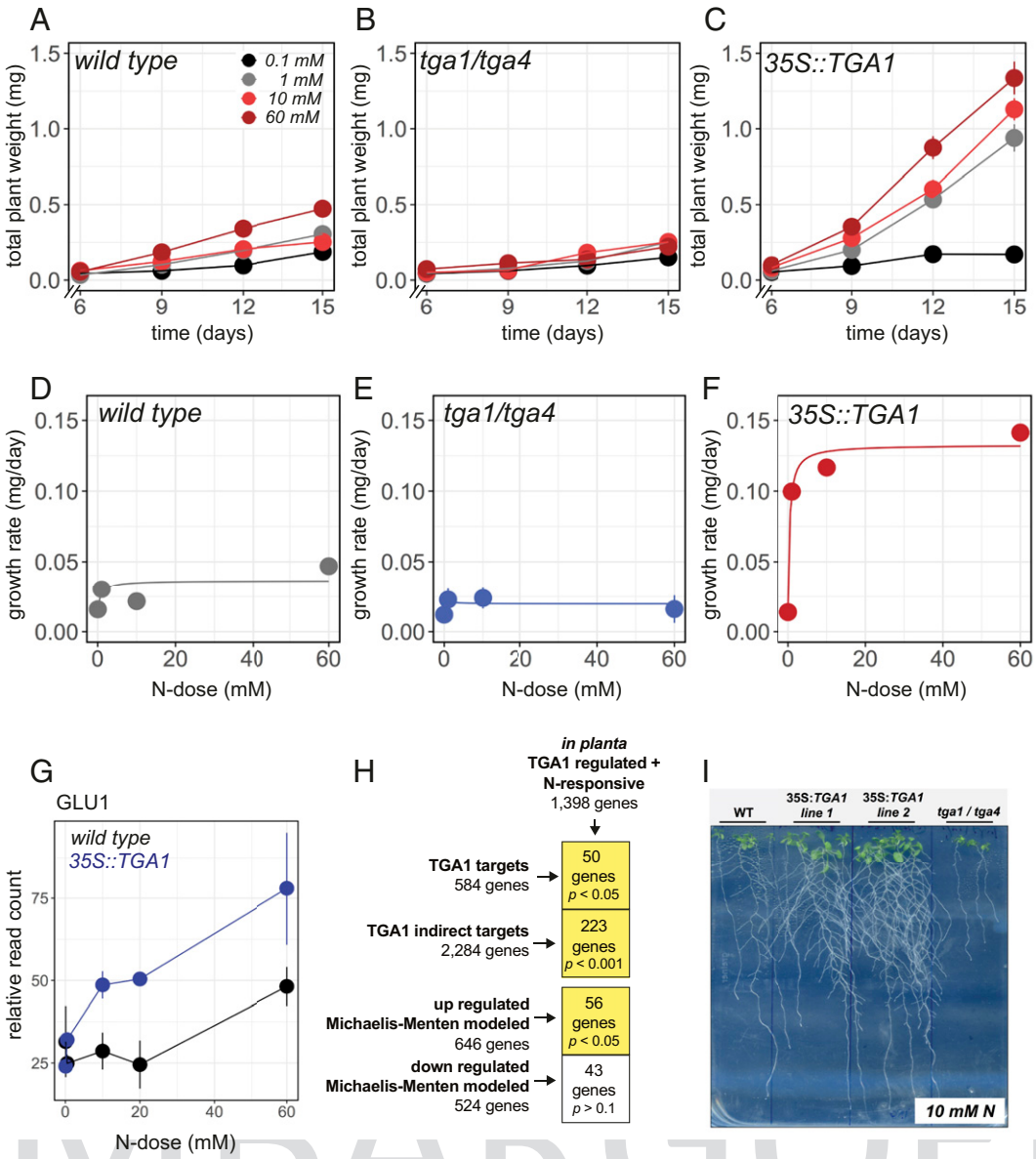

Fig. 4. Changes in TGA1 levels impacts N-dose–responsive growth rates *in planta*. (*A*–*C*) Growth rates of (*A*) wild-type, (*B*) *tga1/tga4*, and (*C*) *35S::*TGA1 seedling growth over time (days) under different N-doses. The impact of N-dose on growth rates differs significantly between wild-type and the *35S::*TGA1 line (three-way ANCOVA, $P = 4.1 \times 10^{-5}$), and between wild-type and the *tga1/tga4* line ($P = 1.5 \times 10^{-7}$). (*D*–*F*) Rates of plant growth of (*D*) wild-type, (*E*) *tga1/tga4*, and (*F*) *35S::*TGA1 plants, fit with the MM model. (*G*) GLU1 gene expression assayed under these N-dose conditions in wild-type and *35S::*TGA1. (*H*) Genes differentially expressed in response to N-dose in *35S::*TGA1 plants significantly intersect with direct and indirect targets of TGA1, as well as MM-modeled genes (Monte Carlo test). (*I*) Phenotype of 15-d-old wild-type plants, a *tga1/tga4* mutant, and two independent TGA1-overexpressing lines grown on plates containing 10 mM N.

expression of some MM-modeled genes occurring even in the absence of TGA1 (i.e., in the *tga1/tga4* mutant background) (Fig. 2*E*). Moreover, according to the MM model, an increase in enzyme concentration in vitro leads to an increase in V_{max}, without a change in K_m (12). Thus, our observation of a change in K_m values in both *tga1/4* mutants and in *35S::*TGA1 (*SI Appendix*, Fig. S7) suggests additional transcriptional or posttranscriptional mechanisms are at play in regulating rates of N-dose gene expression in vivo.

We show that the impact of TGA1 on the rate of transcriptional change in response to N-dose is linked to TGA1's ability to accelerate plant growth (Fig. 4 and *SI Appendix*, Fig. S11). This is supported by our data; a significant portion of genes whose expression can be modeled by MM kinetics in response to N-dose are also differentially expressed in TGA1-overexpressing plants, plants that displayed accelerated growth rates (Fig. 4 and *SI Appendix*, Fig. S11). In this way, TGA1 likely plays a key role in aligning the rate of N uptake with rate of N growth (Fig. 5). For this reason, our findings provide context as to why overexpression of TFs can lead to improvements in plant growth responses. Such a mechanism may be at work in other studies in which overexpression of TFs involved in N signaling have led to improvements in plant N-use efficiency, such as DOF1 and NLP7 (39, 40). For our study, we speculate that the increase in growth rate caused by TGA1 overexpression is due to improvements in N-assimilation efficiency, rather than an increase in N uptake. This is suggested by our TGA1 network, which reveals that TGA1 directly—or indirectly through intermediate TFs—regulates 12 genes involved in N assimilation in root cells, compared to only three genes involved in N transport (Fig. 3*C*). This interpretation is also supported by

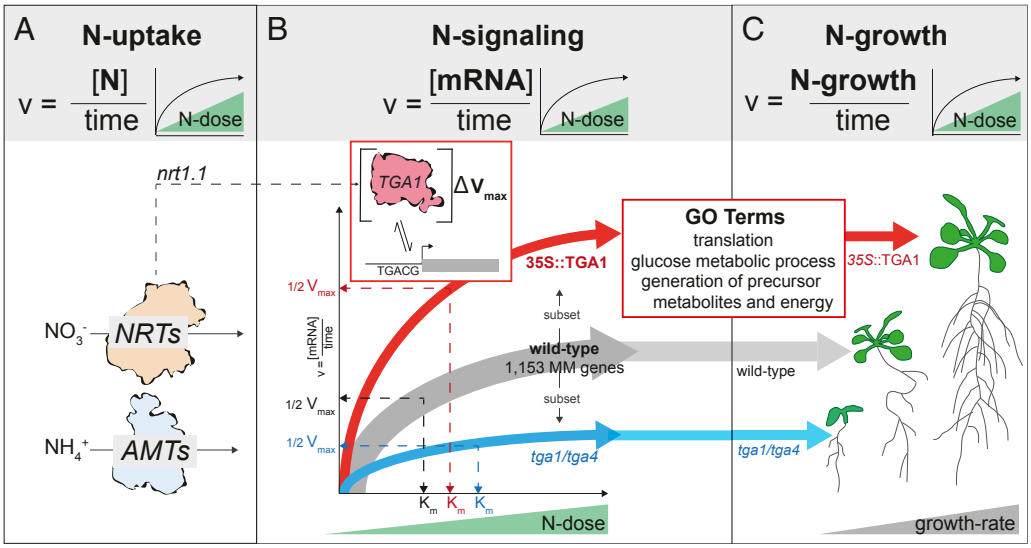

Fig. 5. The molecular basis for Michaelis–Menten (MM) kinetics that underlies N-dose–dependent regulation of plant growth. The MM model (upper gray panel) can explain the effect of N-dose on rates of N uptake (*A*), N signaling (*B*), and N growth (*C*). (*A*) The rate of N uptake by plant nitrate (NRTs) and ammonium (AMTs) transporters follows MM kinetics (11). The N-regulated expression of the NRT1.1 nitrate transceptor has also been shown to follow MM kinetics (53). (*B*) Results presented herein show that transcriptome responses to N-dose follows MM kinetics (1,153 genes) (Fig. 1). Moreover, a portion of this MM-mediated transcriptome response (192 genes) to N-dose is affected by TGA1, as shown via changes in V_{max} and K_m in *tga1/4* and *35S::*TGA1 lines (Figs. 2 and 4 and *SI Appendix*, Fig. S7). TGA1's role in signaling N-dose at the molecular level impacts genes involved in translation, glucose metabolism, and energy metabolism. The N response of TGA1 mRNA levels is altered in the *nrt1.1* transceptor mutant (*SI Appendix*, Fig. S12) (18). (*C*) Overexpression of TGA1 (*35S::*TGA1) leads to higher N-dose–dependent growth rates, while it is reduced in the *tga1/4* mutant (Fig. 4 *D–F*). Thus, the role of TGA1 in mediating rate of transcript change in response to N-dose provides a molecular basis for how N-dose regulates rates of plant growth, a phenotype that can also be explained by MM kinetics (Fig. 4 *D–F*) (10).

previous studies showing that TGA1 regulates genes involved in N metabolism in roots (18, 20), and that N uptake is not perturbed in *tga1/tga4* double mutant (18). However, we note that TGA1's effect on N-dose–responses likely involves more than simply targeting N-assimilation genes. We found evidence that TGA1 regulates the expression of 92 other TFs—agreeing with a previous report showing TGA1 regulates the expression of many N-responsive TFs (20). Consequently, TGA1 does not act alone in regulating N-dose–responses.

Since TGA1's expression itself is responsive to N-dose, it is likely that TGA1 sits downstream of the molecular mechanisms that sense N-dose. One such mechanism is NRT1.1, a nitrate transceptor that allows plants to sense a wide range of nitrate doses, and whose expression is also driven by MM kinetics (33). To test the hypothesis that TGA1 sits downstream of the NRT1.1 nitrate transceptor, we overlapped genes whose expression is dependent on NRT1.1 (41) with genes regulated by TGA1 (20), as well as genes whose expression is modeled by MM kinetics in our study (*SI Appendix*, Fig. S12). The significant overlap between these gene lists suggest that NRT1.1 and TGA1 are in the same pathway that control rates of transcriptional change in response to N-dose (Fig. 5 and *SI Appendix*, Fig. S12).

Our finding that increasing TGA1 mRNA levels results in proportional increases in mRNA of its target genes supports time-based methods that rely on TF mRNA levels to infer TF–target interactions (4, 5, 42, 43). In agreement with this, one recent study that employed time-series mRNA data to infer TF–target interactions used 33 TFs—including TGA1—to experimentally validate the resulting gene-regulatory network (20). In that study, TGA1 mRNA levels were able to predict target gene expression with one of the highest precision rates (75%) of all 33 TFs tested (20).

Finally, our study demonstrates that assaying for rates of transcript change in response to nutrient dose, rather than simply a change in gene expression at one time point, represents a fruitful approach to identify loci of interest. Indeed, this approach could be applied to identify TF regulators of other types of environmental cues in plants or other species. In our case, we identified TGA1, a TF that accelerates plant growth responses to N in part by impacting transcription rates of N-metabolism genes. As such, future work should investigate whether overexpression of TGA1 enhances crop growth in the field. More broadly, our study of the basic mechanisms that underlie the transcriptome kinetics that respond to changes in N-dose has the potential to enhance plant growth rates and improve N-use efficiency.

Materials and Methods

N-Dose-by-Time Factorial Experiment. Approximately 100 seedlings of *Arabidopsis* Col-0, *35S::*TGA1 (sourced from ref. 20) and *tga1/tga4* (sourced from ref. 18) genotypes were grown for 13 d hydroponically on MS media (16), supplemented with 1 mM KNO_3 and 1% sucrose. Light conditions were diurnal (16-h light and 8-h dark), with light intensity 120 $\mu mol \cdot m^{-2} \cdot s^{-1}$ at constant temperature of 22 °C. After 13 d, plants were starved for N for 1 d. After 24 h of N starvation, 2 h after subjective dawn, plants were provided with one of four N-doses, either no N, 0.3 mM KNO_3 + 0.3 mM NH_4NO_3, 3.3 mM KNO_3 + 3.3 mM NH_4NO_3 or 20 mM KNO_3 + 20 mM NH_4NO_3. This created total-N doses of 0, 1, 10, or 60 mM. For each N-dose, N exposure time lasted for one of five time periods: 15, 30, 60, 120, or 240 min. At the respective time point, roots were cut and frozen immediately in liquid nitrogen. Each genotype was tested under each dose–time condition in duplicate.

RNA was extracted from root tissue using the RNeasy Mini Kit (Qiagen) with on-column DNase treatment. RNA quality was assessed using Agilent Tapestation using High Sensitivity RNA ScreenTape. One microgram of total RNA per sample was depleted of rRNA by Thermo Fisher Scientific mRNA Purification Kit. RNA-seq libraries were made using the NEBNext Ultra RNA Library Prep Kit and sequenced using Next Seq Illumina platform with 1×75-bp single read-end chemistry. Reads were then aligned to the *Arabidopsis* TAIR10 genome using Tophat (44), and gene counts called using HT-seq (45) with Araport11 annotation (46). Statistical analyses were then performed in R, as detailed below.

To control for the effect of potassium ions inducing differential expression within our assay, we compared *Arabidopsis* seedlings (Col-0) treated for 240 min with a dose of 20 mM KNO_3 + 20 mM NH_4NO_3 with seedlings treated for 240 min with a mock dose of 20 mM KCl. We found 44 differentially expressed genes due to salt treatment using DESeq2 (47) (adjusted $P < 0.01$). These genes were removed from subsequent analyses.

N-Dose-by-Time Statistical Analysis. Our factorial matrix experiment held two continuous variables—time and N-dose. To capture genes that were differentially expressed by either or both of these factors, we used the following linear model:

$$\text{gene}_a \text{ expression} = \alpha + \beta_1 \text{N} + \beta_2 \text{T} + \beta_3 \text{N} \times \text{T}.$$

The full linear model was fit to the RNA-seq read counts of each gene (implemented in DESeq2 using *design* ~ N + T + N × T), where N and T variables were logged to the base 2. We then performed model simplification as follows:

1) Using the "LRT" command, an adjusted *P* value was computed for each of the factors within the model across all fit genes.
2) If a gene were fit significantly by all three terms (adjusted $P < 0.01$), then this gene was deemed fit by the full model and removed from remaining model simplification steps.
3) For all remaining genes, the factor with the least significance (highest adjusted *P* value) was removed, and the model was refit with the remaining terms. This allows for one of three variations of a simplified model to be fit for each gene.
4) If a gene was fit significantly by two terms (both adjusted *P* values < 0.01), then this gene was deemed fit by a two-term model and removed from remaining model simplification steps.
5) Steps 3 and 4 were repeated fitting one term models.

If a gene was not fit by any model form, then it was removed from further analysis. GO terms were called using VirtualPlant software (48).

To calculate rates of change in transcript abundance of genes at each N-dose, we fit each gene's quantile-normalized expression values using the lm() function in R, using time as the dependent variable. These estimated rates of transcription under each N dose were then fit to the MM model using the drm() function in R. We note that rates were first normalized by subtracting the rate calculated for the 0 mM condition. After this subtraction, we then took the absolute values of each rate, which allowed us to model genes that had decreases in rates of transcription at higher N-doses (conferring to increases in gene repression over N-dose). We calculated the significance of the model by correlating model predicted values with input values (Pearson false-discovery rate-normalized $P < 0.05$). Additionally, we tested whether a simpler model could explain changes in transcription dynamics. We assessed whether any of the 3,818 genes followed first-order kinetics—a model in which the rate of mRNA change is linearly proportional to N-dose. We found no genes that significantly fit this model.

RNA-Seq, 4tU, and ChIP-Seq TARGET TF-Perturbation Experiments. The cell-based TARGET assay for TF perturbation was performed as described in ref. 22 for steady-state mRNA and as in ref. 26 to capture de novo transcripts with 4tU. Briefly, Col-0 or *tga1/tga4* seedlings were grown on vertical plates supplemented with MS media at 1 mM KNO_3 and 1% sucrose under light conditions as described above. After 14 d, 2 h after subjective dawn, plant roots were harvested, finely cut, and placed in protoplast solution for 3 h. Root cell protoplasts were then washed and then PEG mediated transfected with pBOB11_C-term (available through https://gatewayvectors.vib.be/; National Center for Biotechnology Information accession number MN991175), a derivative of the pBeaconRFP_GR TARGET TF expression vector (22), which contains the TGA1-GR fusion protein and a *35S::*RFP gene for selection of transfected cells by fluorescence-activated cell sorting (FACS) (22). Transfected root cells were incubated overnight to express the TF-GR fusion protein. The following day, the root cells were treated 2 h after subjective dawn with N-dose present in standard MS media (20 mM KNO_3 + 20 mM NH_4NO_3), or control 20 mM KCl treatment. Cells were treated with CHX 100 min thereafter, or with a mock treatment of DMSO to enable the identification only of direct targets of the TF. To induce TF-GR localization to the nucleus, cells were treated with DEX 20 min thereafter, or with a mock ethanol treatment. Each treatment combination was tested in triplicate. Treated root cells were incubated for a further 2 h, then successfully transfected cells were FACS purified using RFP expression. To perform 4tU mRNA labeling, we repeated the above experimental treatment on transfected root protoplasts, treating three replicates of transfected root protoplasts with 1.5 mM 4tU in the presence of DEX and CHX, and three replicates in the presence of CHX only (26). All RNA-seq libraries were prepared through purifying polyadenylated transcripts as previously described above, and sequenced using the HiSeq Illumina platform with 1×50-bp single read-end chemistry or Next Seq Illumina platform with 1×75-bp single read-end chemistry.

For ChIP-seq analysis of TF binding, Col-0 seedlings were grown, and root cells were isolated and transfected as described above. Approximately 1 million root cells were treated for 100 min with 20 mM KNO_3 + 20 mM NH_4NO_3, followed by a 20-min treatment with CHX, followed by a treatment of DEX lasting 1 min. Protoplasts were fixed with formaldehyde for 10 min, and then treated with 2 M glycine for 5 min, before being flash frozen in liquid nitrogen. ChIP was performed on samples as outlined in ref. 28, using an anti-GR antibody (GR P-20; Santa Cruz Biotechnology; 200 μg/mL). ChIP-seq libraries were made using NEBNext Ultra II DNA Library Prep Kit and sequenced using Next Seq Illumina platform with 1×75-bp single read-end chemistry.

TARGET RNA-Seq Statistical Analysis. To find direct targets of TGA1, we implemented a three-way ANODEV model on our +CHX RNA-seq datasets in DESeq2 with *design* ~ N + DEX + biological replicate. To find genes directly regulated by TGA1 in the presence of CHX, we took those genes that were significantly differentially expressed due to DEX treatment using the contrast function (adjusted *P* value < 0.01). To control for the effects of CHX on gene expression, we performed a two-way ANODEV model on our –CHX RNA-seq dataset, using *design* ~ N + DEX. In this way, we found those genes that were significantly differentially expressed due to DEX treatment in the absence of CHX (adjusted *P* value < 0.01). We deemed a gene a direct target of TGA1 if it was differentially expressed due to DEX-induced TF nuclear import in both +CHX and –CHX conditions. A gene was deemed an indirect TARGET of TGA1 if it was found to be regulated in response to DEX-induced TF nuclear import only in the absence of CHX. GO terms were called using VirtualPlant software (48).

ChIP-Seq Analysis. Reads obtained from the ChIP DNA and Input DNA were filtered and aligned to the *Arabidopsis thaliana* genome (TAIR10) using Bowtie2 (49), where clonal reads were removed. The ChIP alignment data were compared to its partner Input DNA and peaks were called using MACS2 (q = 0.05) (50). These regions were overlapped with the genome annotation to identify genes within 2 kbp downstream of the peak using Bedtools (*SI Appendix*, Table S5) (51). Genome browser images were made using the Integrative Genomics Viewer (52).

Plant Biomass Phenotyping. *Arabidopsis* seedlings—Col-0, *35S*::TGA1 (line 1), 35S:TGA1 (line 2), and *tga1/tga4*—were grown on vertical plates. Light and temperature conditions were identical to those described above. Plants were grown on MS media, with total N concentrations 0.1, 1, 10, and 60 (where N was supplied as KNO_3 + NH_4NO_3). Total plant dry weight was measured 6, 9, 12, and 15 d after sowing.

Steady-State Transcriptomics. *Arabidopsis* seedlings Col-0 and *35S::*TGA1, were grown on vertical plates for 15 d on 0.1, 0.5, 10, 20, or 60 mM N KNO_3 + NH_4NO_3. Root tissue was then flash frozen and sequenced as described previously. To discover differentially expressed genes, we fit an ANODEV model in DESeq2 (using *design* ~ Genotype + $\log_2$Nitrogen). We used genes that were found differentially expressed in response to both $\log_2$Nitrogen and Genotype factors to intersect with other gene sets. The significance of intersects were assessed using Monte Carlo simulations (10,000 iterations), using the intersect of differentially expressed genes within each dataset as background.

Data Availability. The data and R code that support the findings of this study are available from the corresponding author upon reasonable request. Raw sequencing data can be found at the National Center for Biotechnology Information Sequence Read Archive (accession number PRJNA522060).

ACKNOWLEDGMENTS. This work was supported by a grant on Plant Genomics to G.M.C. from the Zegar Family Foundation (A16-0051), the Beachell-Borlaug International Scholarship to J.S., and grants to G.M.C. from the National Science Foundation (NSF) (NSF–Plant Genome Research Program Grants IOS-1339362 and NSF-DBI-0445666). We thank Joan Doidy for providing pBOB11_C-term vector, and Laurie Leonelli for critical reading of the manuscript.

1. Y. Y. Wang, P. K. Hsu, Y. F. Tsay, Uptake, allocation and signaling of nitrate. *Trends Plant Sci.* **17**, 458–467 (2012).
2. D. Breitburg *et al*., Declining oxygen in the global ocean and coastal waters. *Science* **359**, eaam7240 (2018).
3. J. Canales, T. C. Moyano, E. Villarroel, R. A. Gutiérrez, Systems analysis of transcriptome data provides new hypotheses about *Arabidopsis* root response to nitrate treatments. *Front Plant Sci* **5**, 22 (2014).
4. G. Krouk, P. Mirowski, Y. LeCun, D. E. Shasha, G. M. Coruzzi, Predictive network modeling of the high-resolution dynamic plant transcriptome in response to nitrate. *Genome Biol.* **11**, R123 (2010).
5. K. Varala *et al*., Temporal transcriptional logic of dynamic regulatory networks underlying nitrogen signaling and use in plants. *Proc. Natl. Acad. Sci. U.S.A.* **115**, 6494–6499 (2018).
6. K. Patterson *et al*., Distinct signalling pathways and transcriptome response signatures differentiate ammonium- and nitrate-supplied plants. *Plant Cell Environ.* **33**, 1486–1501 (2010).

7. R. Wang *et al*., Genomic analysis of the nitrate response using a nitrate reductase-null mutant of *Arabidopsis*. *Plant Physiol.* **136**, 2512–2522 (2004).
8. J. Swift, M. Adame, D. Tranchina, A. Henry, G. M. Coruzzi, Water impacts nutrient dose responses genome-wide to affect crop production. *Nat. Commun.* **10**, 1374 (2019).
9. X. S. Yang *et al*., Gene expression biomarkers provide sensitive indicators of in planta nitrogen status in maize. *Plant Physiol.* **157**, 1841–1852 (2011).
10. R. Lana *et al*., Application of Lineweaver–Burk data transformation to explain animal and plant performance as a function of nutrient supply. *Livest. Prod. Sci.* **98**, 219–224 (2005).
11. G. G. McNickle, J. S. Brown, When Michaelis and Menten met Holling: Towards a mechanistic theory of plant nutrient foraging behaviour. *AoB Plants* **6**, plu066 (2014).
12. L. Menten, M. I. Michaelis, Die kinetik der invertinwirkung. *Biochem. Z.* **49**, 333–369 (1913).
13. L. Michaelis, M. L. Menten, K. A. Johnson, R. S. Goody, The original Michaelis constant: Translation of the 1913 Michaelis–Menten paper. *Biochemistry* **50**, 8264–8269 (2011).
14. N. van Uden, Transport-limited fermentation and growth of *Saccharomyces cerevisiae* and its competitive inhibition. *Arch. Mikrobiol.* **58**, 155–168 (1967).
15. S. López *et al*., A generalized Michaelis–Menten equation for the analysis of growth. *J. Anim. Sci.* **78**, 1816–1828 (2000).
16. T. Murashige, F. Skoog, A revised medium for rapid growth and Bio assays with tobacco tissue cultures. *Physiol. Plant.* **15**, 473–497 (1962).
17. G. Rubin, T. Tohge, F. Matsuda, K. Saito, W. R. Scheible, Members of the LBD family of transcription factors repress anthocyanin synthesis and affect additional nitrogen responses in *Arabidopsis*. *Plant Cell* **21**, 3567–3584 (2009).
18. J. M. Alvarez *et al*., Systems approach identifies TGA1 and TGA4 transcription factors as important regulatory components of the nitrate response of *Arabidopsis thaliana* roots. *Plant J.* **80**, 1–13 (2014).
19. M. L. Gifford, A. Dean, R. A. Gutierrez, G. M. Coruzzi, K. D. Birnbaum, Cell-specific nitrogen responses mediate developmental plasticity. *Proc. Natl. Acad. Sci. U.S.A.* **105**, 803–808 (2008).
20. M. D. Brooks *et al*., Network Walking charts transcriptional dynamics of nitrogen signaling by integrating validated and predicted genome-wide interactions. *Nat. Commun.* **10**, 1569 (2019).
21. O. Titiz *et al*., PDX1 is essential for vitamin B6 biosynthesis, development and stress tolerance in *Arabidopsis*. *Plant J.* **48**, 933–946 (2006).
22. B. O. R. Bargmann *et al*., TARGET: A transient transformation system for genome-wide transcription factor target discovery. *Mol. Plant* **6**, 978–980 (2013).
23. N. Yamaguchi, C. M. Winter, F. Wellmer, D. Wagner, Identification of direct targets of plant transcription factors using the GR fusion technique. *Methods Mol. Biol.* **1284**, 123–138 (2015).
24. A. Para *et al*., Hit-and-run transcriptional control by bZIP1 mediates rapid nutrient signaling in *Arabidopsis*. *Proc. Natl. Acad. Sci. U.S.A.* **111**, 10371–10376 (2014).
25. C. Lindermayr, S. Sell, B. Müller, D. Leister, J. Durner, Redox regulation of the NPR1-TGA1 system of *Arabidopsis thaliana* by nitric oxide. *Plant Cell* **22**, 2894–2907 (2010).
26. J. Doidy *et al*., "Hit-and-Run" transcription: De novo transcription initiated by a transient bZIP1 "hit" persists after the "run." *BMC Genomics* **17**, 92 (2016).
27. M. D. Cleary, C. D. Meiering, E. Jan, R. Guymon, J. C. Boothroyd, Biosynthetic labeling of RNA with uracil phosphoribosyltransferase allows cell-specific microarray analysis of mRNA synthesis and decay. *Nat. Biotechnol.* **23**, 232–237 (2005).
28. A. Para, Y. Li, G. M. Coruzzi, μChIP-Seq for genome-wide mapping of in vivo TF-DNA interactions in *Arabidopsis* root protoplasts. *Methods Mol. Biol.* **1761**, 249–261 (2018).
29. R. C. O'Malley *et al*., Cistrome and epicistrome features shape the regulatory DNA landscape. *Cell* **165**, 1280–1292 (2016).
30. D. Yan *et al*., NIN-like protein 8 is a master regulator of nitrate-promoted seed germination in *Arabidopsis*. *Nat. Commun.* **7**, 13179 (2016).
31. Y. Liu, X. Li, K. Li, H. Liu, C. Lin, Multiple bHLH proteins form heterodimers to mediate CRY2-dependent regulation of flowering-time in Arabidopsis. *PLoS Genet* **9**, e1003861 (2013).
32. P. Shannon *et al*., Cytoscape: A software environment for integrated models of biomolecular interaction networks. *Genome Res.* **13**, 2498–2504 (2003).
33. C. H. Ho, S. H. Lin, H. C. Hu, Y. F. Tsay, CHL1 functions as a nitrate sensor in plants. *Cell* **138**, 1184–1194 (2009).
34. I. Nachman, A. Regev, N. Friedman, Inferring quantitative models of regulatory networks from expression data. *Bioinformatics* **20** (suppl. 1), i248–i256 (2004).
35. I. H. Segel, Enzyme kinetics: Behavior and analysis of rapid equilibrium and steady state enzyme systems. *FEBS Lett.* **60**, 102–103 (1975).
36. A. Gaudinier *et al*., Transcriptional regulation of nitrogen-associated metabolism and growth. *Nature* **563**, 259–264 (2018).
37. E. A. Vidal *et al*., Nitrate-responsive miR393/AFB3 regulatory module controls root system architecture in *Arabidopsis thaliana*. *Proc. Natl. Acad. Sci. U.S.A.* **107**, 4477–4482 (2010).
38. A. Honkela *et al*., Genome-wide modeling of transcription kinetics reveals patterns of RNA production delays. *Proc. Natl. Acad. Sci. U.S.A.* **112**, 13115–13120 (2015).
39. L. H. Yu *et al*., Overexpression of Arabidopsis NLP7 improves plant growth under both nitrogen-limiting and -sufficient conditions by enhancing nitrogen and carbon assimilation. *Sci. Rep.* **6**, 27795 (2016).
40. S. Yanagisawa, A. Akiyama, H. Kisaka, H. Uchimiya, T. Miwa, Metabolic engineering with Dof1 transcription factor in plants: Improved nitrogen assimilation and growth under low-nitrogen conditions. *Proc. Natl. Acad. Sci. U.S.A.* **101**, 7833–7838 (2004).
41. E. Bouguyon *et al*., Multiple mechanisms of nitrate sensing by *Arabidopsis* nitrate transceptor NRT1.1. *Nat. Plants* **1**, 15015 (2015).
42. P. Mirowski, Y. LeCu, "Dynamic factor graphs for time series modeling" in *Machine Learning and Knowledge Discovery in Databases*, W. Buntine, M. Grobelnik, D. Mladenic, J. Shawe-Taylor, Eds. (Springer, Berlin, 2009), vol. 2, pp. 128–143.
43. G. Krouk, J. Lingeman, A. M. Colon, G. Coruzzi, D. Shasha, Gene regulatory networks in plants: Learning causality from time and perturbation. *Genome Biol.* **14**, 123 (2013).
44. C. Trapnell, L. Pachter, S. L. Salzberg, TopHat: Discovering splice junctions with RNA-seq. *Bioinformatics* **25**, 1105–1111 (2009).
45. S. Anders, P. T. Pyl, W. Huber, HTSeq—a Python framework to work with high-throughput sequencing data. *Bioinformatics* **31**, 166–169 (2015).
46. C. Y. Cheng *et al*., Araport11: A complete reannotation of the *Arabidopsis thaliana* reference genome. *Plant J.* **89**, 789–804 (2017).
47. M. I. Love, W. Huber, S. Anders, Moderated estimation of fold change and dispersion for RNA-seq data with DESeq2. *Genome Biol.* **15**, 550 (2014).
48. M. S. Katari *et al*., VirtualPlant: A software platform to support systems biology research. *Plant Physiol.* **152**, 500–515 (2010).
49. B. Langmead, S. L. Salzberg, Fast gapped-read alignment with Bowtie 2. *Nat. Methods* **9**, 357–359 (2012).
50. Y. Zhang *et al*., Model-based analysis of ChIP-seq (MACS). *Genome Biol.* **9**, R137 (2008).
51. A. R. Quinlan, I. M. Hall, BEDTools: A flexible suite of utilities for comparing genomic features. *Bioinformatics* **26**, 841–842 (2010).
52. H. Thorvaldsdóttir, J. T. Robinson, J. P. Mesirov, Integrative genomics viewer (IGV): High-performance genomics data visualization and exploration. *Brief. Bioinform.* **14**, 178–192 (2013).
53. H. C. Hu, Y. Y. Wang, Y. F. Tsay, AtCIPK8, a CBL-interacting protein kinase, regulates the low-affinity phase of the primary nitrate response. *Plant J.* **57**, 264–278 (2009).